Influence of Area Ratio and Chloride Concentration on the Galvanic Coupling of Copper and Carbon Steel

JES Focus Issue on Advanced Techniques in Corrosion Science in Memory of Hugh Isaacs

Influence of Area Ratio and Chloride Concentration on the Galvanic Coupling of Copper and Carbon Steel

Thalia E. Standish,[1,*] Lindsay J. Braithwaite,[1,*] David W. Shoesmith,[1,2,] and James J. Noël[1,2,***,z]**

[1] *Department of Chemistry, The University of Western Ontario, London, Ontario N6A 5B7, Canada*
[2] *Surface Science Western, London, Ontario N6G 0J3, Canada*

Carbon steel (CS) vessels coated with ~3 mm of Cu have been proposed for the permanent disposal of used nuclear fuel in a deep geological repository (DGR) in Canada. In the event of an undetected defect in the Cu coating that exposes the underlying CS to groundwater, the possibility of galvanically accelerated corrosion of CS arises. In this work, the impact of O_2 availability, NaCl solution concentration, and cathode:anode area ratio on the galvanic corrosion behavior of Cu/CS couples was evaluated by monitoring the galvanic potential of the couple and the galvanic current passing between Cu and CS. The corrosion products and surface damage were analyzed using Raman spectroscopy and SEM/EDX. Varying the Cu:CS area ratio from 1:1 to 2500:1, the [Cl^-] from 0.001 to 3.0 M, the sparging gas from air to Ar, and monitoring the resulting changes in the galvanic current, galvanic potential, corrosion products, and surface damage showed that the galvanic corrosion of CS was most severe when it was exposed to air-sparged solution with a moderate [Cl^-] (0.1 M) as part of the couple with the largest Cu:CS area ratio.
 [DOI: 10.1149/2.0521911jes]

Manuscript submitted March 25, 2019; revised manuscript received June 11, 2019. Published June 27, 2019. *This paper is part of the JES Focus Issue on Advanced Techniques in Corrosion Science in Memory of Hugh Isaacs.*

Canada's plan for the permanent disposal of used nuclear fuel involves sealing the used fuel bundles in Cu-coated carbon steel (CS) containers and placing them in a multi-barrier system in a deep geological repository (DGR).[1–4] The Cu coating (~3 mm–thick) provides corrosion protection, while the CS inner vessel provides the necessary mechanical strength. In the unlikely event that a through-coating defect goes undetected and the underlying CS is exposed to groundwater, galvanic corrosion could occur. Cu, being more noble, would act as the cathode (with O_2 reduction as the primary cathodic reaction), while CS would experience accelerated corrosion as the anode (Fe oxidation).[5–9] It is judicious to evaluate what would happen in such a scenario.

In general, the extent of galvanic coupling will depend on the properties of the materials, their geometry relative to one another, and the exposure environment. In the context of the Cu-coated CS containers, the critical factors are the amount of O_2 available, the cathode:anode area ratio and the composition of the groundwater (which may be modified by radiolysis products and by the clay barrier that will be present at the container surface in a DGR). The concern is that if a though-coating defect were to go undetected during inspection of the container, a small exposed area of CS would be surrounded by a large area of Cu, which could result in an extremely high current density (and corrosion rate) on the exposed CS. However, the distance over which the CS anode can couple to the Cu cathode will depend on the dissolved [O_2], the O_2 diffusion coefficient, and the ionic strength of the environment (an electrolyte must be present for any galvanic corrosion to occur). The amount of O_2 available to drive corrosion will also depend on how much is consumed by other oxidation processes in a DGR. In addition, the transport of species to the container surface will be limited by the surrounding clay barrier and by corrosion products that may form, which will further limit the corrosion rate.

Previous studies have been conducted on Cu-coated CS samples with a simulated through-coating defect exposed to 3.0 M NaCl solution, where corrosion damage was monitored and characterized using X-ray micro-computed tomography (micro-CT) and electrochemical and spectroscopic techniques.[4,8,9] While these studies are essential for evaluating the extent of corrosion and the damage morphology at a through-coating defect, the galvanic current, I_g, cannot be measured when Cu is in direct contact with CS. Separating Cu and CS and connecting them through a zero-resistance ammeter (ZRA) enables the measurement of I_g, which provides an additional measure of the extent of galvanic coupling and the rate of corrosion. Several researchers have used this configuration to investigate the galvanic coupling behavior of Cu and CS or cast iron in a variety of exposure environments relevant to DGR conditions.[6,7,10,11] However, there remains a need for a systematic evaluation of how the galvanic corrosion behavior of a Cu/CS couple will change over the range of conditions that are possible in a DGR.

The conditions in a DGR will evolve over time from oxic, dry, and warm to anoxic, wet, and cool, and the composition of groundwater will vary depending on the location of the DGR. In Canada, the [Cl^-] in groundwater ranges from 0 to 5 M and numerous other solutes may also be present;[12,13] it is not currently known exactly how the different Cl^- concentrations will affect the galvanic corrosion between Cu and CS. In addition, it is prudent to determine how through-coating defects of different sizes (i.e., different cathode:anode area ratios) would affect corrosion. One previous study evaluated Cu/mild steel couples with area ratios of 10:1, 1:1, and 1:10 in aerated seawater,[14] but the dependence of galvanic corrosion on a wider range of Cu/CS area ratios remains unknown. The effective cathode:anode area ratio under DGR conditions may also be influenced by the conductivity of the groundwater and the effects of the consolidated porous medium (bentonite clay) in contact with container surfaces, both of which could be considered in the context of "throwing power" around the defect. Higher temperatures may accelerate the corrosion processes but will also decrease the solubility of O_2. Although this factor is not considered in the present study, it has been researched previously for Cu/cast iron and Cu/CS couples in deaerated environments.[6,7]

In this work, we manipulate a selection of the aforementioned conditions, specifically the [O_2], [Cl^-], and Cu:CS area ratio, to investigate their individual and combined influence on the galvanic corrosion behavior of CS coupled to Cu. To reflect the geometry of a through-coating defect and to minimize the influence of asymmetrical geometry on the results, the electrodes were designed such that a cylinder of CS is situated inside a ring of Cu as they are immersed together in an electrolyte. The two electrodes are insulated from being in direct contact with one another but are electrically connected through a ZRA. The galvanic current, I_g, and galvanic potential, E_g, are monitored and the surface damage and

*Electrochemical Society Student Member.
**Electrochemical Society Fellow.
***Electrochemical Society Member.
[z]E-mail: jjnoel@uwo.ca

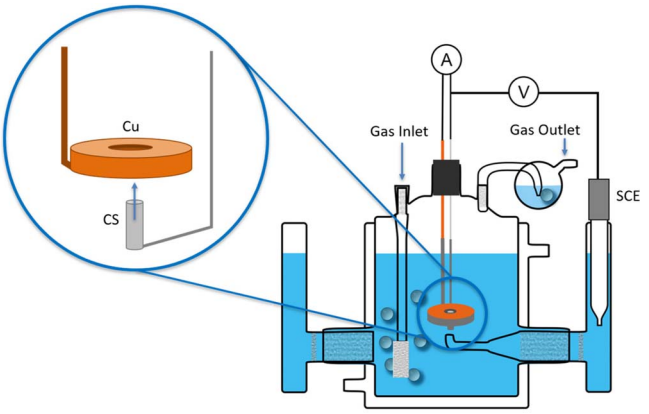

Figure 1. Illustration of the electrochemical cell and electrode design.

corrosion products are characterized using scanning electron microscopy (SEM)/energy dispersive X-ray spectroscopy (EDX) and Raman spectroscopy.

Experimental

Experiments were conducted using A516 Grade 70 carbon steel (CS) provided by the Nuclear Waste Management Organization (NWMO) and P-doped (30–100 ppm), O-free Cu provided by the Swedish Nuclear Fuel and Waste Management Co. (SKB). The CS was cut into cylindrical electrodes of varying diameter and the Cu was cut into rings of varying outer and inner diameter. After the electrodes were wet-ground to a P1200 finish with SiC paper, a wire was soldered onto the back side of each of the electrodes, PTFE heat-shrink tubing was applied to insulate the wire, and the electrodes were sonicated in methanol. Three layers of Amercoat epoxy paint (PPG Protective & Marine Coatings) were applied to the electrodes, leaving the top surface exposed, and each coat was cured at 60°C for 24 hours. The exposed electrode surface was wet-ground to a P2500 finish with SiC paper and sonicated in methanol prior to beginning each experiment. The surface area of the CS electrodes ranged from 0.004 to 1.0 cm^2 and the Cu rings were 1.0 and 10.0 cm^2. By varying the size combination of the Cu and CS electrodes, Cu:CS area ratios ranging from 1:1 to ∼2500:1 were achieved.

As illustrated in Figure 1, the cylindrical CS electrode was placed in the center of the Cu ring to reduce geometrical influences on the galvanic corrosion measurements, and the electrodes were immersed in an Ar- or air-sparged NaCl solution (concentration ranging from 0.001 to 3.0 M) in a three-compartment electrochemical cell. The solution was prepared with reagent grade NaCl (Fisher Scientific) and ultrapure water from a Thermo Scientific Barnstead Nanopure water purification system set to yield a resistivity of 18.2 MΩ·cm. The solution was sparged with either ultra high purity Ar (PRAXAIR) for ∼60 minutes or medical grade air (PRAXAIR) for ∼30 minutes before starting an experiment, and sparging continued throughout the experiment. The CS and Cu electrodes were connected through a ZRA (Keithley 6514 system electrometer with National Instruments Labview software written in-house), enabling us to measure the galvanic current, I_g, flowing between them. The galvanic current density, i_g, was calculated by dividing the steady-state I_g by the surface area of CS. The potential of the couple, E_g, was monitored using a potentiostat (Solartron Model 1480 Multistat with CorrWare software) which was connected to the CS electrode and a saturated calomel reference electrode (SCE). Each experiment was terminated when E_g and I_g reached steady-state conditions. Couples with Cu:CS area ratios of 1:1 and 10:1 tended to take longer to reach steady-state, 2–7 days, while the couples with larger area ratios stabilized more quickly; 100:1 couples were stable after ∼30 h (although periodic fluctuations were still observed) and couples ≥500:1 were stable within 4–20 h. After each experiment ended, the electrodes were removed from solution, rinsed with ultrapure water (taking care not to disturb the corrosion products), and stored in an anaerobic chamber. Potentiodynamic polarization curves were recorded on Cu and CS electrodes by scanning −0.550 V and +0.250 V, respectively, from the corrosion potential (E_{corr}) at a scan rate of 10 mV min^{-1}, using Pt foil as the counter electrode. The polarizations were initiated once E_{corr} reached steady-state.

Surface analysis was performed at Surface Science Western using SEM/EDX (Hitachi SU3500 Variable Pressure SEM combined with an Oxford AZtec X-Max50 SDD X-ray analyzer) and Raman spectroscopy (Renishaw InVia Reflex Raman Spectrometer with a 633 nm laser wavelength).

Results

Electrochemical measurements.—The potentiodynamic polarization curves for CS and Cu exposed to air-sparged 3.0 M and 0.1 M NaCl solutions are shown in Figure 2. For both conditions, the anodic branch (corresponding to the oxidation of Fe to Fe^{2+}) is shown for CS, and the cathodic branch (corresponding to the reduction of O_2) is shown for Cu. The intersection point between the anodic and cathodic branches provides an estimate of the galvanic current density (i_g) and the galvanic potential (E_g) that Cu and CS will adopt once they are coupled together. The intersection point of the two branches occurs at 48 μA cm^{-2} and −0.644 V_{SCE} in 3.0 M NaCl solution and at 140 μA cm^{-2} and −0.630 V_{SCE} in 0.1 M NaCl solution. Decreasing the concentration from 3.0 M to 0.1 M NaCl results in a substantial increase in the current response and E_{corr} of Cu, but almost no change in the polarization behavior of CS. In both conditions, Cu is polarized far from its E_{corr}, indicating that O_2 reduction on Cu is the rate-determining reaction.

Plotting the measured i_g and E_g of Cu/CS couples exposed to 0.1 M and 3.0 M NaCl solutions sparged with either air or Ar, as a function of Cu:CS area ratio, Figure 3, shows the influence of [O_2], area ratio, and [Cl^-]. In Ar-sparged 3.0 M NaCl solutions, i_g and E_g are significantly lower than in aerated solutions, and increasing the Cu:CS area ratio from 1:1 to 100:1 has a minor effect on i_g and E_g; i_g increases from 2.0 to 4.6 μA cm^{-2} and E_g increases by 30 mV. In comparison, in air-sparged conditions, increasing the Cu:CS area ratio from 1:1 to 100:1 significantly affects i_g and E_g; i_g increases ∼100-fold and E_g increases by 100−200 mV. Overall, as the Cu:CS area ratio increases in the presence of O_2, both i_g and E_g tend to increase, although there is some deviation from this behavior at the largest area ratios. The value of i_g is ∼30 μA cm^{-2} at a 1:1 area ratio and increases in proportion to the area ratio at approximately the same rate in both 0.1 M and 3.0 M NaCl solutions E_g is initially between −0.666 and −0.677 V_{SCE} at the smallest area ratio and rises at a slightly faster rate in 0.1 M NaCl solution than it does in 3.0 M solution. At the largest area ratios, E_g is −0.313 V_{SCE} and −0.422 V_{SCE} in 0.1 M and 3.0 M NaCl solutions, respectively. To provide a basis for comparison, the corrosion potential, E_{corr}, of an uncoupled CS specimen was measured in aerated 3.0 M and 0.1 M NaCl solutions; the steady-state E_{corr} values were −0.687 V_{SCE} and −0.655 V_{SCE}, respectively.

Decreasing the [Cl^-] from 3.0 M to 0.1 M tends to result in an increase in i_g and E_g for a given area ratio; i_g as much as doubles, although for area ratios of 100:1 and ∼1000:1 i_g remains almost the same. The difference between E_g values in 3.0 M and 0.1 M NaCl solutions is only 11 mV at the 1:1 area ratio, and the difference grows to over 100 mV at the largest area ratios. Further decreasing the [Cl^-] to 10 mM and 1 mM results in a decrease in i_g and an increase in E_g, as seen in the plots of i_g and E_g vs [Cl^-], Figure 4. In addition, at lower [Cl^-] (10 mM), the difference between the i_g of the 100:1 and 10:1 couples diminishes, and at the lowest [Cl^-] (1 mM), there is almost no difference between the i_g of couples with the two area ratios.

Surface analysis.—SEM/EDX analysis of the CS samples corroded in Ar-sparged solutions shows some damage to the surface and almost no deposition of corrosion products. The damage is a combination of uniform corrosion (with some preferential corrosion of certain grains) and pit-like features, some of which are centered around

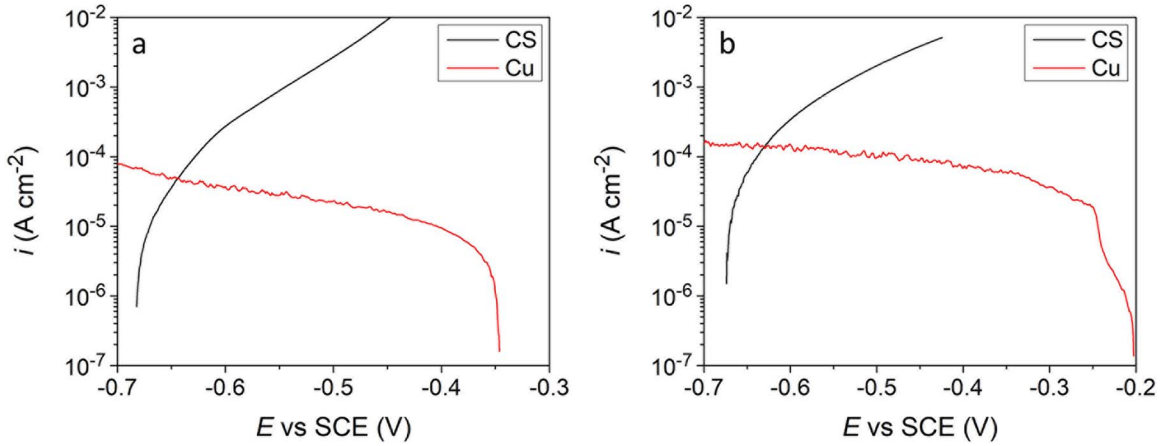

Figure 2. Potentiodynamic polarization behavior of CS and Cu exposed to air-sparged (a) 3.0 M and (b) 0.1 M NaCl solutions.

particles that typically have a higher Al and O content, and sometimes a higher S and Cu content, than the surrounding CS according to EDX, Figure 5. Looking at the surface under higher magnification by SEM, Figure 6, shows that certain grains have experienced uniform corrosion, while others appear raised and have a lamellar structure. EDX mapping shows that these raised grains have a higher carbon content than the surrounding area, Figures 5a and 5e, and the Raman spectra from these grains, spectra 1 and 2 in Figure 7, show a very broad band between ~1300 and 1600 cm^{-1}, which can be attributed to residual Fe_3C.[15–17] Very broad and weak Raman bands are present below 500 cm^{-1} and around 700 cm^{-1} in some spectra, which suggests that some Fe^{III} or Fe^{II}/Fe^{III} oxide/oxyhydroxide may be on the surface.

CS electrodes that were part of couples with area ratios from 1:1 to 500:1 and exposed to air-sparged 3.0 M or 0.1 M NaCl are covered with many corrosion product deposits. Raman spectra of the corrosion products show that they are a mix of Fe^{III} and Fe^{II}/Fe^{III} oxides and oxyhydroxides; Figure 8 shows representative spectra from each of the different species identified in these corrosion product deposits. The most frequently identified species are γ-FeOOH, based on the series of sharp peaks below 700 cm^{-1}, with the most intense at 252 cm^{-1} and the second most intense at 380 cm^{-1}, Figure 8 spectrum 1, and γ-Fe_2O_3, based on the broad peak between ~665 and 730 cm^{-1}, Figure 8 spectrum 2.[18–20] Fe_3O_4 and α-FeOOH are also present, based on peaks at 670 cm^{-1}, Figure 8 spectra 3 and 4, and 385–390 cm^{-1}, Figure 8 spectrum 5, respectively, but appear less frequently.[18,19] Figure 8 spectrum 3 also has contributions from γ-Fe_2O_3 and possibly other Fe^{III} oxyhydroxides, judging by the small, broad peaks and higher intensity of the baseline below 600 cm^{-1}. Many of the other Raman spectra recorded on the CS electrodes that were part of couples with area ratios from 1:1 to 500:1 and exposed to air-sparged 3.0 M or 0.1 M NaCl (not presented here) exhibit a combination of the aforementioned peaks, indicating that the corrosion products are composed of a mix of Fe^{III} and Fe^{II}/Fe^{III} oxides and oxyhydroxides. Although many Fe^{III} species were produced, the pH of the solution did not change significantly over the duration of the experiment, indicating that the solution has some buffering capability. SEM images show more severe damage to the CS surface at larger Cu:CS ratios, Figure 9, and less corrosion product formation/deposition. At area ratios of 1000:1 and greater, the species identified by Raman spectroscopy on CS are residual Fe_3C and γ-Fe_2O_3; the signal from residual Fe_3C is particularly intense on these samples, Figure 10. The Fe_3C signature is also seen in the Raman spectra from CS surfaces that were part of 100:1 and 500:1 area ratio couples exposed to 3.0 M and 0.1 M NaCl.

Raman spectra recorded on the CS electrodes from the 10:1 and 100:1 couples exposed to 1 mM NaCl solution, Figure 11, show that the surface is covered in patches of γ-FeOOH (spectra 1 and 7), Fe_3O_4 (spectra 2–5, 8, and 9), and γ-Fe_2O_3 (spectra 4–6 and 10), with traces of green rust (spectrum 11). Green rust is a Fe^{II}-Fe^{III} hydroxy-salt and was identified based on the peaks at ~430 and 505 cm^{-1}, spectrum 11 in Figure 11c, which are attributed to Fe^{2+}—OH and Fe^{3+}—OH stretching modes in green rust.[21–23] The small peak at ~218 cm^{-1} (ref. 219–221 cm^{-1}) is likely due to the presence of Cl^- within the green rust structure.[23] Each Raman spectrum tends to have peaks for only one, or sometimes two, species, indicating that the corrosion products are not as mixed as on the CS electrodes that were part of couples exposed to higher Cl^- concentrations. Fe_3O_4 was identified more frequently

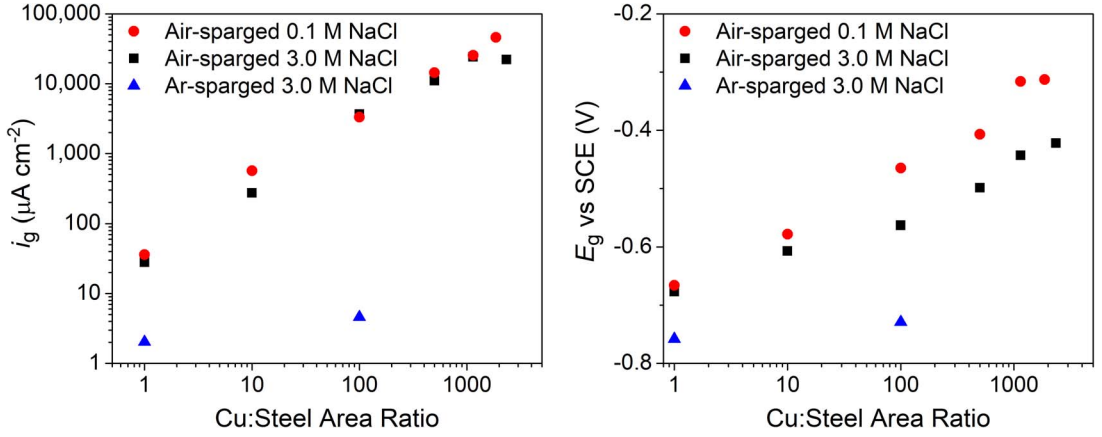

Figure 3. Galvanic current density (i_g) and galvanic potential (E_g) of Cu/CS couples exposed to 0.1 M and 3.0 M NaCl solutions sparged with either air or Ar, as a function of Cu:CS area ratio (normalized so CS = 1).

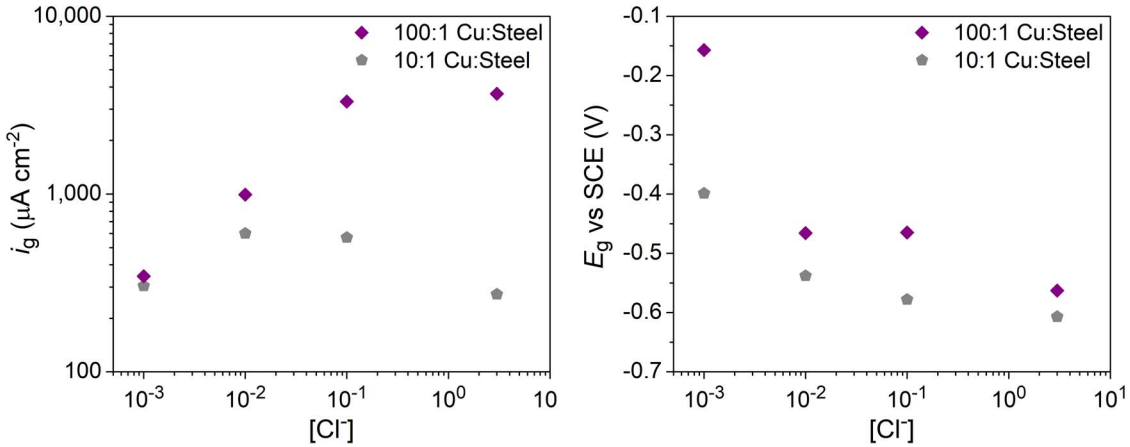

Figure 4. i_g and E_g for 100:1 and 10:1 Cu:CS couples exposed to NaCl solutions ranging from 1 mM to 3.0 M.

on the CS electrodes exposed to 1 mM NaCl solution than on those exposed to higher Cl^- concentrations, suggesting that Fe_3O_4 is more predominant in 1 mM NaCl.

On all but four of the corroded CS samples, EDX shows the presence of Cu, which ranges from 0.6 to 28.2 wt%. In all cases, Cu is associated with the CS surface, where corrosion products had been either dislodged or not deposited, Figure 12. All of the samples on which no Cu is detected are completely covered with corrosion products, so any underlying Cu would be obscured. Peaks for Cu_2O were also identified in some of the Raman spectra acquired from the corroded CS specimens based on the very broad peak centered around 620 cm^{-1} (e.g. Figure 7 spectrum 5).[24,25] No Cu was detected by EDX on samples exposed to 1 mM NaCl solution, but as the [Cl^-] increased, so too did the average amount of Cu detected. To determine the origin of the Cu, two additional experiments were performed: one in which CS was corroded in air-sparged 0.1 M NaCl in the absence of a Cu electrode and another in which CS and Cu were galvanically coupled but immersed in separate solutions that were connected by a salt bridge. In both cases, 0.3–1.4 wt% Cu was detected on the CS surfaces by EDX after corrosion. This indicates that Cu originating in the CS itself can accumulate on the CS surface as corrosion occurs (the CS used has a Cu content of 0.01 wt%), however it does not account for the much higher amounts of Cu observed on some of the CS electrodes from the galvanic coupling experiments where Cu and CS were immersed together.

Discussion

Influence of O_2.—In the presence of O_2, galvanic coupling with Cu enhances the corrosion rate of CS, based on i_g measurements (Figure 3), which show significant current passing between Cu as the cathode and CS as the anode, and surface analyses, which show that CS is heavily corroded while little to no damage occurs on Cu. This behavior is expected, since O_2 reduction on Cu is the driving force behind the galvanically accelerated corrosion of CS. Removing the dissolved O_2 removes this driving force and there is almost no coupling between Cu and CS (some coupling occurred in the Ar-sparged experiments in this work, based on the non-zero i_g, which was likely due to trace dissolved O_2 present in the solution). The more negative E_g values observed under Ar-sparged conditions are indicative of a less oxidizing environment and are consistent with the E_{corr} values of uncoupled CS exposed to Ar-sparged 4.0 M NaCl solution, −0.772 V_{SCE},[26] and 5.0 M NaCl solution, ∼−0.710 to −0.770 V_{SCE}.[17] The minor impact that increasing the Cu:CS area ratio has on i_g and E_g in Ar-sparged conditions compared to air-sparged conditions supports a conclusion

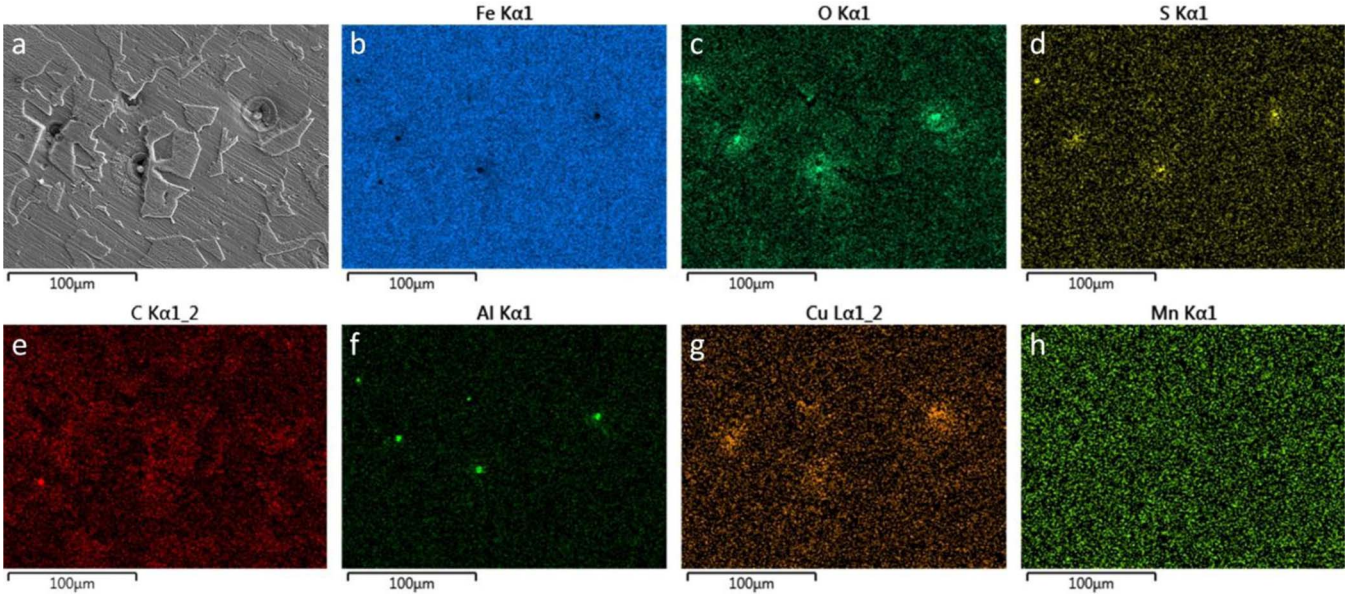

Figure 5. (a) SEM image and (b-h) EDX maps recorded on CS exposed to Ar-sparged 3.0 M NaCl solution as part of a 100:1 couple.

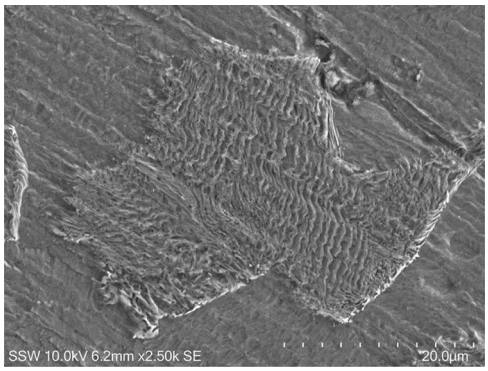

Figure 6. SEM image recorded on the surface of a CS sample exposed to Ar-sparged 3.0 M NaCl solution for 45 h as part of a 100:1 couple.

that galvanic coupling with Cu does not play a significant role in accelerating the corrosion of CS in the absence of O_2.

Previous research has also shown that in deaerated conditions the corrosion rate of cast iron coupled to Cu is close to the corrosion rate of uncoupled cast iron.[6,10] The authors also noted that although the corrosion rate is initially determined by the kinetics of the cathodic reaction (H_2 evolution reaction), the corrosion rate decreases over time due to the corrosion product film that forms on the cast iron surface.[6,10] The lack of corrosion products on CS exposed to Ar-sparged conditions in this work is likely due to the short duration of the experiments (43–45 h). The raised lamellar structure (Figure 6) and higher carbon content of certain grains seen by SEM/EDX, along with the Fe_3C signature between ~1300 and 1600 cm^{-1} in the Raman spectra from these grains, indicate that this corrosion damage morphology is the result of preferential corrosion of the α-ferrite bands from pearlite grains leaving behind the Fe_3C bands.[15–17] This behavior has been seen previously on CS exposed to Ar-sparged and N_2-sparged solutions;[17,27] Fe_3C can act as a preferential cathode, thereby driving anodic dissolution of the α-ferrite. The more uniformly corroded grains are likely α-ferrite.

Influence of cathode:anode area ratio.—A larger Cu:CS (cathode:anode) area ratio results in a greater i_g in air-sparged conditions (Figure 3), which corresponds to a higher corrosion rate. At a 1:1 area ratio, i_g is ~28 µA cm^{-2} in 3.0 M NaCl solution and ~36 µA cm^{-2} 0.1 M NaCl solution. A similar value, 27.4 µA cm^{-2}, was measured

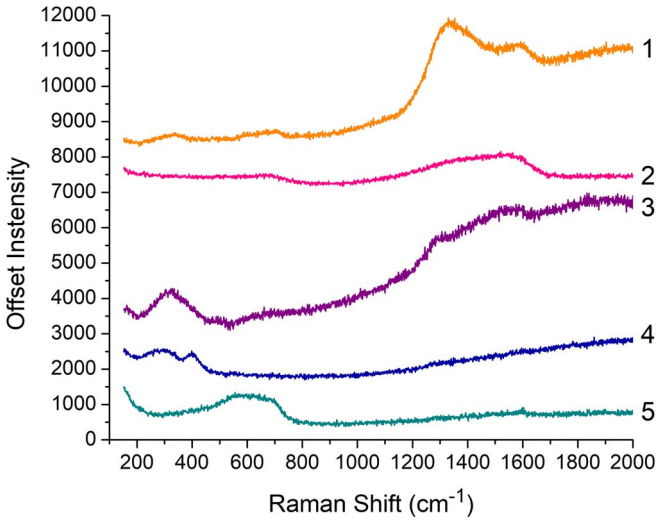

Figure 7. Raman spectra recorded on CS exposed to Ar-sparged 3.0 M NaCl solution as part of a 100:1 couple.

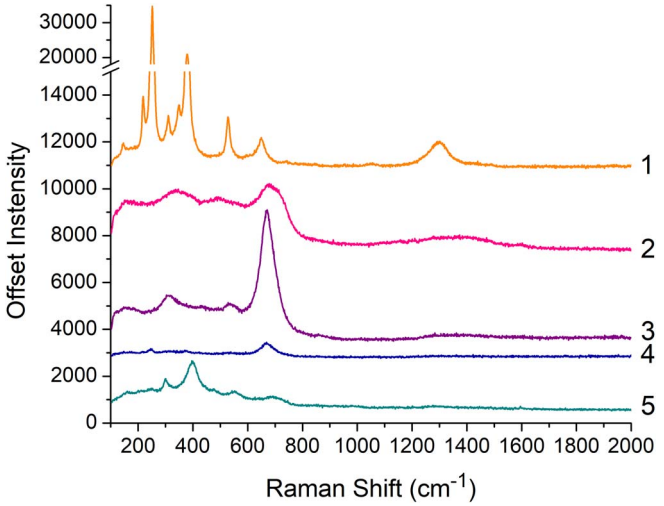

Figure 8. Representative Raman spectra recorded on CS surfaces that were exposed to air-sparged 3.0 M or 0.1 M NaCl as part of area ratios from 1:1 to 500:1.

by Mansfeld and Kenkel on a Cu/CS couple exposed to naturally aerated 0.6 M NaCl solution over 24 hours.[11] The increase in i_g with increasing Cu:CS area ratio indicates that the galvanic corrosion rate is under cathodic control (i.e., the galvanic corrosion rate is limited by the rate at which O_2 can be reduced on Cu), since the galvanic current, I_g, is dictated by the Cu surface area and is independent of the CS surface area. The rate of the O_2 reduction reaction is under either diffusion or mixed control (not activation control, based the results from previous research),[28] but additional studies are needed to determine which. Given that the net current on the anode (I_a) and on the cathode (I_c) must be equal in magnitude at E_g, as the area of CS decreases relative to the Cu area, the same magnitude of I_a must be supported on a smaller area, resulting in a higher current density on CS (higher i_g). This proportional dependence of i_g on the cathode:anode area ratio in aerated conditions has been observed on other galvanic couples[29,30] and has been described mathematically.[31] Weight loss measurements have also shown that the severity of galvanic corrosion of mild steel increases with an increase in the Cu:steel area ratio in aerated seawater, although the range of area ratios in this study was limited to 10:1, 1:1, and 1:10.[14] The present results extend the experimental data to include larger cathode:anode area ratios.

The logarithmic increase in E_g to less negative values is consistent with the known logarithmic relationship between E_g and cathode:anode area ratio.[31–33] At small Cu:CS area ratios, CS is not polarized far from its corrosion potential (E_{corr}), which was −0.655 V_{SCE} in aerated 0.1 M NaCl solution, so both oxidation and reduction reactions can occur on the CS surface at an appreciable rate.[31] This also means that the measured i_g is smaller than the actual anodic current density on CS (which would be equal to the sum of the cathodic currents on Cu and CS). Increasing the Cu:CS area ratio polarizes CS further from its

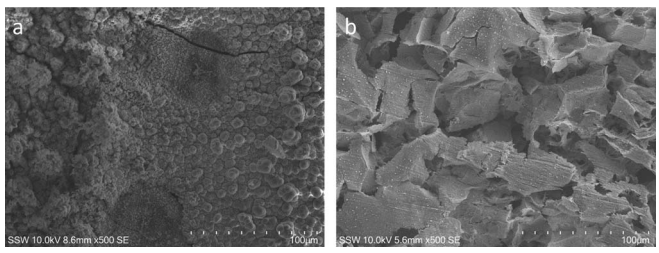

Figure 9. SEM images recorded on the surface of CS samples exposed to air-sparged 0.1 M NaCl solution for (a) 130 h as part of a 100:1 couple and (b) 6 h as part of a ~1000:1 couple.

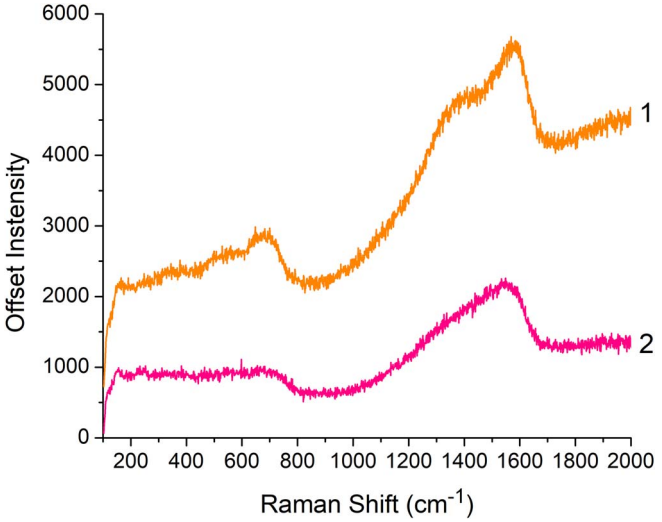

Figure 10. Raman spectra recorded on CS electrodes from >1000:1 couples exposed to 0.1 M NaCl solution.

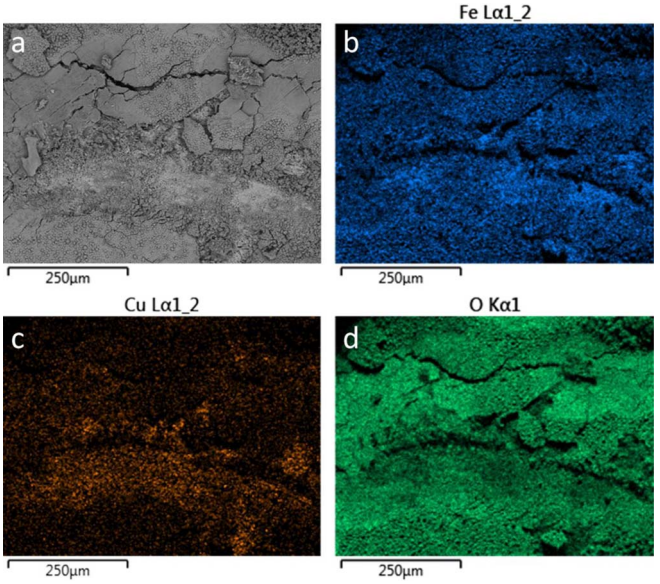

Figure 12. (a) SEM image and (b-d) EDX maps recorded on CS exposed to air-sparged 0.1 M NaCl solution as part of a 500:1 couple, illustrating the presence of Cu on CS.

E_{corr}, toward the more noble E_{corr} of Cu. Above an area ratio of ~100:1, CS is most likely polarized far enough from its E_{corr} such that no appreciable reduction occurs on CS and the measured i_g is equivalent to the anodic current density.[34] The deviation from the growth trends of i_g and E_g at the largest area ratio in 3.0 M NaCl solution may be due to the anodic reaction on CS becoming partially rate controlling.

The more severe damage seen in the SEM images as the area ratio increases (Figure 9) is consistent with the higher i_g values and is another indication of higher corrosion rates. The presence of a Fe_3C signature in the Raman spectra recorded on CS from couples with area ratios ≥100:1 is indicative of corrosion of pearlite grains in the CS. The smaller amount of corrosion products on the CS surface at greater area ratios may be due to the shorter duration of the experiments. The higher rate of O_2 consumption when the surface area of the Cu electrode is greater may also contribute to decreasing the deposition of corrosion products, since with less O_2 available, soluble ferrous species would not be as readily oxidized to insoluble corrosion products. In addition, if the soluble Fe species migrate far enough from the CS surface before they are oxidized, which can occur more easily as the CS surface area becomes smaller, the corrosion products would not deposit onto the CS surface but would precipitate and fall to the bottom of the electrochemical cell.

Influence of [Cl⁻].—The higher i_g and less negative E_g values in 0.1 M NaCl solution compared to those obtained in 3.0 M NaCl solution (Figure 3) are in agreement with the predicted trends in i_g and E_g from the potentiodynamic polarization curves (Figure 2). The predicted E_g values from the polarization results are slightly less negative (by ~35 mV) than the measured values for a couple with a 1:1 area ratio, although the magnitude of the increase in E_g (+14 mV) when [Cl^-] is decreased from 3.0 M to 0.1 M is close to the magnitude of the increase observed experimentally (+11 mV). The measured i_g is only slightly lower than the predicted value in 3.0 M NaCl solution (28 μA cm^{-2} and 48 μA cm^{-2}, respectively), although in 0.1 M NaCl solution, the measured i_g is substantially lower than the measured value (36 μA cm^{-2} and 140 μA cm^{-2}, respectively). This significant difference may indicate that there are additional factors influencing the i_g of the Cu/CS galvanic couple that are not accounted for when Cu and CS are tested individually in potentiodynamic polarization experiments, such as the conductivity of the solution and the potential and current distributions across the galvanic couple.

The higher i_g and less negative E_g values in 0.1 M NaCl solution (Figure 3) can be attributed, at least in part, to the higher solubility of O_2 in 0.1 M (~7.6 wt ppm at 22°C)[35] compared to 3.0 M NaCl solution (~2.8 wt. ppm at 22°C).[36] With more dissolved O_2 in solution, the environment is more oxidizing and, given that O_2 reduction on Cu is

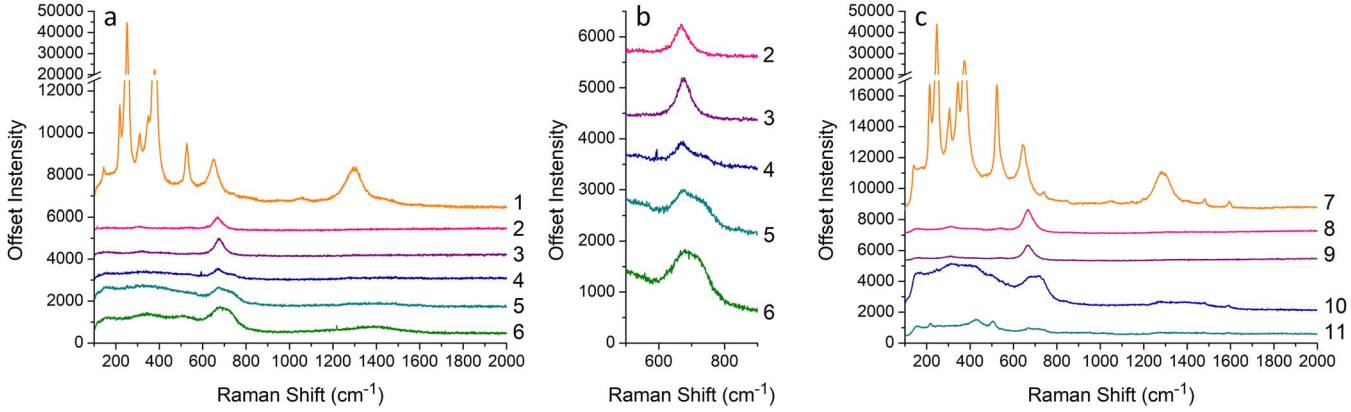

Figure 11. Raman spectra recorded on CS electrodes from the (a) 10:1 couple, with (b) showing detail of the peaks between 600 and 800 cm^{-1}, and the (c) 100:1 couple, both exposed to 1 mM NaCl solution.

the rate-determining reaction, the driving force for corrosion is greater (i.e., there is more O_2 available to be reduced, driving Fe oxidation), which explains the increased i_g and E_g. A higher concentration of dissolved O_2 could also result in a larger $[O_2]$ gradient, which would increase the flux of O_2 to the surface and, thereby, the corrosion rate. In addition, the diffusivity of O_2 in NaCl solution increases slightly with decreasing $[Cl^-]$;[37,38] which can also contribute to increasing the flux of O_2 to the surface. O_2 is ~2.7 times more soluble in 0.1 M NaCl than in 3.0 M NaCl at 22°C, so one would expect a corresponding increase in i_g. However, the measured i_g is only 1−2 times greater in 0.1 M NaCl, indicating that although O_2 plays a critical role in determining the galvanic corrosion rate, other factors influence i_g. One such factor could be the conductivity of the 0.1 M NaCl solution, 1.07×10^4 $\mu S\ cm^{-1}$, which is an order of magnitude lower than that of 3.0 M NaCl solution, 2.05×10^5 $\mu S\ cm^{-1}$.[39] Lower solution conductivity can result in less uniform current and potential distributions across the electrodes, and a higher solution resistance (R) leads to a lower current for a given potential difference, because of the ohmic (IR) drop.[32,40]

While lowering the $[Cl^-]$ from 3.0 M to 0.1 M results in increases in i_g and E_g, decreasing it further to 10 mM and then 1 mM results in a continued increase in E_g but a decrease in i_g (Figure 4), indicating a decrease in the anodic reaction rate (i.e., a lower Fe oxidation rate). The decreasing difference between the i_g values of the 100:1 and 10:1 couples as the $[Cl^-]$ is decreased from 10 mM to 1 mM demonstrates that the conductivity of the solution, which is 1.18×10^3 and 124 $\mu S\ cm^{-1}$ for 10 and 1 mM NaCl solutions, respectively,[39] is not high enough to enable coupling between the CS and the entire Cu area available. At these low $[Cl^-]$, even though O_2 is more soluble than at 3.0 M or 0.1 M NaCl, i_g does not continue to increase, which supports the suggestion that the low conductivity of the solution limits the distance over which O_2 reduction on Cu can couple to Fe oxidation on CS (the "throwing power"). The formation of a protective oxide on CS would explain the significant increase in E_g at 1 mM $[Cl^-]$. The strong presence of Fe_3O_4 seen by Raman spectroscopy may be indicative of partial passivation of the CS surface, since it tends to form a compact layer that is not ionically conductive and therefore prevents oxidation of the underlying steel. In addition, unlike other CS specimens that were part of 10:1 or 100:1 couples in higher $[Cl^-]$ conditions, no Fe_3C signature is seen in the Raman spectra for CS from the couples in 1 mM NaCl solution, indicating that the CS surface is less damaged, which is in agreement with SEM images and the relatively low i_g and high E_g.

Overall, considering the influence of $[Cl^-]$ on the Cu/CS galvanic couple, there is a balance between the conductivity of the solution and the O_2 solubility. At very low Cl^- concentrations, the low solution conductivity restricts the distance over which CS and Cu can couple. Increasing the $[Cl^-]$ increases the conductivity of the solution, which allows CS to couple to a greater area of Cu and results in a greater corrosion rate. However, increasing the $[Cl^-]$ also decreases the solubility of O_2, which results in a lower corrosion rate. This means that the greatest galvanic corrosion rates can occur at moderate Cl^- concentrations, likely between 0.1 and 3 M.

Cu accumulation on CS.—Regarding the presence of Cu on most of the CS electrodes, although up to 1.4 wt% Cu was detected on a CS surface that was corroded in the absence of Cu, the mechanism by which greater amounts of Cu, up to 28.2 wt%, accumulate on CS is uncertain. Thermodynamically, Cu is stable at the measured E_g values at a dissolved $[Cu_{(aq)}]_{total}$ of 1 μM. However, as $[Cl^-]$ increases and $[Cu_{(aq)}]_{total}$ decreases, the equilibrium potential between Cu and Cu^I chloride complexes (such as $CuCl_2^-$ and $CuCl_3^{2-}$) decreases to close to the measured E_g values, meaning that it would be thermodynamically possible for Cu to corrode. Dissolved Cu chloride complexes could subsequently be reduced on CS, resulting in the observed Cu on CS. The presence of Cu_2O and CuO identified by Raman spectroscopy on some of the corroded CS specimens confirms the presence of Cu and indicates that if Cu had been deposited onto CS in its metallic form (which is not Raman active), some amount of oxidation had subsequently occurred. The definite reason for the appearance of Cu on CS has yet to be proven.

Conclusions

The impact of the degree of aeration, the cathode:anode area ratio, and the $[Cl^-]$ on the galvanic corrosion behavior of Cu/CS couples was assessed by monitoring the i_g and E_g of the couples and by analyzing the surface damage and corrosion products. In the absence of O_2, galvanic coupling with Cu has a negligible influence on the corrosion rate of CS. In aerated conditions, as the cathode:anode (Cu:CS) area ratio increases from 1:1 to ~2500:1, i_g, and therefore the corrosion rate of the CS, increases. i_g increases proportionally with area ratios >~10:1, while at 1:1 Cu:CS and at the highest area ratios in 3.0 M NaCl solution, i_g is lower than would be expected for a linear relationship. The competing effects of $[Cl^-]$ and $[O_2]$ are observed when the $[Cl^-]$ is changed; the $[Cl^-]$ influences both the conductivity and O_2 solubility (as well as the O_2 flux) in the solution, so the extent of galvanic corrosion can be limited by the low solution conductivity at low $[Cl^-]$ and by the low O_2 solubility and reduced O_2 flux at high $[Cl^-]$. In relation to a used nuclear fuel container, the most damage to CS could occur at a small through-coating defect (i.e., large cathode:anode) that is exposed to groundwater with a moderate $[Cl^-]$, likely between 0.1 and 3.0 M, during the initial oxic stage of a DGR. However, the extent of galvanic corrosion may be influenced by other factors such as additional groundwater solutes, solution radiolysis products, temperature, and the clay transport barrier that will be in contact with the Cu-coated container in a DGR. These factors will be the subjects of future studies. In addition, a finite element model of the Cu/CS galvanic couple is currently in development, which will aid in examining the current and potential distributions in this system.

Acknowledgments

This research is jointly funded by the Nuclear Waste Management Organization (NWMO), Toronto and the Natural Sciences and Engineering Research Council of Canada (NSERC) under a Collaborative Research and Development grant (CRDPJ 507465 – 16). Assistance provided by personnel at Western University's Engineering Machine Shop, Chemistry Department, and Surface Science Western is gratefully acknowledged.

ORCID

Thalia E. Standish https://orcid.org/0000-0001-6102-4135
James J. Noël https://orcid.org/0000-0003-3467-4778

References

1. D. S. Hall and P. G. Keech, *Corros. Eng. Sci. Technol.*, **52**, 2 (2017).
2. P. G. Keech, P. Vo, S. Ramamurthy, J. Chen, R. Jacklin, and D. W. Shoesmith, *Corros. Eng. Sci. Technol.*, **49**, 425 (2014).
3. C. H. Boyle and S. A. Meguid, *Nucl. Eng. Des.*, **293**, 403 (2015).
4. T. Standish, J. Chen, R. Jacklin, P. Jakupi, S. Ramamurthy, D. Zagidulin, P. Keech, and D. Shoesmith, *Electrochim. Acta*, **211**, 331 (2016).
5. S. D. Cramer and B. S. Covino, Jr., Eds., *ASM Handbook: Vol. 13A, Corrosion: Fundamentals, Testing, and Protection*, p. 913, ASM International, Materials Park, Ohio (2003).
6. N. R. Smart, A. P. Rance, and P. A. H. Fennel, *TR-05-06 Galvanic corrosion of copper-cast iron couples*, p. 78, Stockholm, Sweden (2005).
7. J. Stoulil, M. Kouřil, L. Pavlova, D. Dobrev, and J. Gondolli, *Mater. Corros.*, **69**, 1163 (2018).
8. T. E. Standish, D. Zagidulin, S. Ramamurthy, P. G. Keech, J. J. Noël, and D. W. Shoesmith, *Corros. Eng. Sci. Technol.*, **52**, 65 (2017).
9. T. E. Standish, D. Zagidulin, S. Ramamurthy, P. G. Keech, D. W. Shoesmith, and J. J. Noël, *Geosciences*, **8**, 360 (2018).
10. N. R. Smart, P. Fennell, A. P. Rance, and L. O. Werme, in *Prediction of Long Term Corrosion Behaviour in Nuclear Waste Systems, Proceedings of the 2nd International Workshop, Eurocorr 2004*. p. 52−60 ANDRA, Nice, France (2004).
11. F. Mansfeld and J. V. Kenkel, *CORROSION*, **31**, 298 (1975).

12. G. M. Kwong, *Status of Corrosion Studies for Copper Used Fuel Containers Under Low Salinity Conditions*, NWMO TR-2011-14; NWMO (2011).
13. J. R. Scully and M. Edwards, *Review of the NWMO Copper Corrosion Allowance*, NWMO TR-2013-04; NWMO, Toronto, ON (2013).
14. D. J. Astley and I. R. Scholes, *Bimetallic Corrosion in Seawater, SMCC/7/74*, Technical report 5/74; Imperial Metal Industries for UK MoD (1974).
15. X.-X. Bi, B. Ganguly, G. P. Huffman, F. E. Huggins, M. Endo, and P. C. Eklund, *J. Mater. Res.*, **8**, 1666 (1993).
16. L. J. Simpson and C. A. Melendres, *J. Electrochem. Soc.*, **143**, 2146 (1996).
17. S. Hill, *thesis*, The University of Western Ontario (2016).
18. M. Hanesch, *Geophys. J. Int.*, **177**, 941 (2009).
19. F. Froment, A. Tournié, and P. Colomban, *J. Raman Spectrosc.*, **39**, 560 (2008).
20. M. Bouchard and D. C. Smith, *Spectrochim. Acta - Part A Mol. Biomol. Spectrosc.*, **59**, 2247 (2003).
21. N. Boucherit, A. Hugot-Le Goff, and S. Joiret, *Corros. Sci.*, **32**, 497 (1991).
22. N. Boucherit and A. Hugot-Le Goff, *Faraday Discuss.*, **94**, 137 (1992).
23. S. Simard, M. Odziemkowski, D. E. Irish, L. Brossard, and H. Ménard, *J. Appl. Electrochem.*, **31**, 913 (2001).
24. J. C. Hamilton, J. C. Farmer, and R. J. Anderson, *J. Electrochem. Soc.*, **133**, 739 (1986).
25. F. Texier, L. Servant, J. L. Bruneel, and F. Argoul, *J. Electroanal. Chem.*, **446**, 189 (1998).
26. C. T. Lee, Z. Qin, M. Odziemkowski, and D. W. Shoesmith, *Electrochim. Acta*, **51**, 1558 (2006).
27. C. T. Lee, M. S. Odziemkowski, and D. W. Shoesmith, *J. Electrochem. Soc.*, **153**, B33 (2006).
28. F. King, M. . Quinn, and C. . Litke, *J. Electroanal. Chem.*, **385**, 45 (1995).
29. F. Mansfeld and J. V. Kenkel, *Corros. Sci.*, **15**, 239 (1975).
30. M. J. Pryor and D. S. Keir, *J. Electrochem. Soc.*, **104**, 269 (1957).
31. F. Mansfeld, *Corrosion*, **27**, 436 (1971).
32. W. H. Smyrl and J. S. Newman, *J. Electrochem. Soc.*, **123**, 1423 (1976).
33. K. B. Oldham and F. Mansfeld, *J. Appl. Electrochem.*, **2**, 183 (1972).
34. F. Mansfeld, *Corrosion*, **29**, 403 (1973).
35. R. Battino, Ed., *Solubility Data Ser.*, **7** (1981).
36. S. D. Cramer, *Ind. Eng. Chem. Process Des. Dev.*, **19**, 300 (1980).
37. M. Jamnongwong, K. Loubiere, N. Dietrich, and G. Hébrard, *Chem. Eng. J.*, **165**, 758 (2010).
38. G. W. Hung and R. H. Dinius, *J. Chem. Eng. Data*, **17**, 449 (1972).
39. P. Vanýsek, in *CRC Handbook of Chemistry and Physics*, 99th Ed. *(Internet Version 2018)*, J. R. Rumble, Editor, CRC Press/Taylor & Francis, Boca Raton, FL.
40. X. G. Zhang, in *Uhlig's Corrosion Handbook*, vol. **13**, p. 210 (2003).